Journal of Catalysis 273 (2010) 29–38

Contents lists available at ScienceDirect

Journal of Catalysis

journal homepage: www.elsevier.com/locate/jcat

NO evolution reaction with NO_2 adsorption over Fe/ZSM-5: In situ FT-IR observation and relationships with Fe sites

Masaoki Iwasaki *, Hirofumi Shinjoh

Toyota Central R&D Laboratories Inc., 41-1 Yokomichi, Nagakute, Aichi 480-1192, Japan

ARTICLE INFO

Article history:
Received 8 March 2010
Revised 26 April 2010
Accepted 27 April 2010

Keywords:
Selective catalytic reduction
NO
NO_2
Zeolite
Fe
Reaction mechanism
FT-IR
Temperature-programmed desorption

ABSTRACT

The evolution of NO following NO_2 introduction onto various Fe/ZSM-5 catalysts was investigated. The activity depended on the method of catalyst preparation used. The most efficient method was CVD with high-Fe loading. Results from in situ FT-IR revealed that NO was initially generated on ion-exchanged Fe sites, temporarily adsorbed, and then desorbed. For the most active samples, the result of temperature-programmed desorption of NO_2, from which ion-exchanged sites may be estimated, indicated that the amount of NO evolution corresponded to nearly half the amount of exchanged Fe. Assuming that most of the exchange sites in these samples are binuclear structures, it may be postulated that one NO molecule evolves from each binuclear site. From this, we propose that NO_2 is decomposed into NO and atomic oxygen at the binuclear Fe sites. The oxygen occupies a bridging vacancy site between Fe atoms. NO evolves and is replaced by follow-on NO_2.

1. Introduction

The adsorption and desorption of NO_x (NO and NO_2), as well as the reduction of NO_x by other molecules, have attracted a great deal of attention in recent years due to their importance in the catalytic removal of NO_x from automotive exhaust. Transition-metal-exchanged zeolites possess properties highly suitable for the adsorption or reduction of NO_x in an oxygen-rich environment, while NH_3 or urea (which is decomposed into NH_3) is a good choice for selective catalytic reduction (SCR) of NO_x due to its high activity and selectivity [1–3].

As is the case for the NH_3-SCR catalysts, Fe-loaded ZSM-5-type zeolite (Fe/ZSM-5) is the most attractive material from the point of view of harmless metal usage, durability at high temperatures, and poisoning [2,4,5]. In addition to SCR reactions, Fe/ZSM-5 has also been investigated extensively for its utility in selective HC oxidation [6–10] and N_2O decomposition [11–14]. Due to these advantages, many physicochemical techniques [3,6,8,9,11,14–16] and computational simulations [17–19] have been performed to better characterize the active Fe sites on zeolites. Although several Fe species have been proposed (isolated, binuclear, and oligonuclear), their precise role in the catalytic reactions remains an ongoing debate, and hence a more detailed physicochemical characterization is warranted.

A typical NH_3-SCR catalytic process is based on the following reaction (so-called standard SCR):

$$NO + NH_3 + 1/2O_2 \rightarrow 2N_2 + 3H_2O \quad (1)$$

In contrast, when NO_2 is contained in the feed, an equimolar NO–NO_2 reaction (so-called fast SCR) occurs that is more highly favored (faster) than the standard SCR reaction (1) [20,21]:

$$NO + NO_2 + 2NH_3 \rightarrow 2N_2 + 3H_2O \quad (2)$$

The fast SCR reaction (2) has played a vital role in helping to meet increasingly stringent regulations for diesel emission. Recently, we have revealed that under fast SCR conditions, both NO_2 and NH_3 possess comparable properties, and thus compete for active adsorption sites on Fe/ZSM-5 [21,22]. For this reason, fast SCR has peculiar properties not shared by standard SCR, which affects transient reaction behavior in addition to the steady-state reaction rate [21]. Thus, NO_2 performs a critical function in controlling the SCR reactions.

Furthermore, NO_2 also plays an important role as a molecular probe for examining active sites. In our laboratory, we found that temperature-programmed desorption (TPD) of NO_2 enables us to estimate the number of ion-exchanged Fe sites (probably including isolated and binuclear) [23]. Using this technique, we were able to derive relationships between the number of Fe sites and the

* Corresponding author. Fax: +81 561 63 6712.
E-mail address: iwasaki@mosk.tytlabs.co.jp (M. Iwasaki).

0021-9517/$ - see front matter © 2010 Elsevier Inc. All rights reserved.
doi:10.1016/j.jcat.2010.04.023

standard SCR performance [23]. Thus, NO_2-TPD represents a robust method for evaluating and quantifying active sites in Fe/zeolite catalysts.

Interestingly, previous studies on the NO_2 adsorption reaction have revealed a concomitant release of NO immediately following NO_2 adsorption over Cu/ZSM-5 [24] and over Fe/ZSM-5 [20,25]. This evolution of NO that follows introduction of NO_2 onto the zeolite surface is a phenomenon also observed for nonzeolite systems such as BaO/Al_2O_3 [26,27]. In many of these systems, one NO molecule is generated for every three NO_2 molecules consumed [20,24–27]. Using BaO/Al_2O_3, the following reaction could explain these findings [26,27]:

$$3NO_2 + BaO \rightarrow Ba(NO_3)_2 + NO \quad (3)$$

The NO_2 adsorption step is a simple yet important process in the fast SCR reaction and in other environmental catalytic reactions such as NO_x storage and reduction (NSR) [26,27] and soot oxidation by NO_2 [28]. In particular, the adsorption behavior of NO_2 over Fe/ZSM-5 has drawn considerable interest, because its mechanism helps us understand the overall de-NO_x kinetics as well as active Fe states and time-scale changes of adsorbates.

In this work, we investigated the NO evolution reaction that takes place on Fe/ZSM-5 zeolites prepared using different methods and with varying Fe content. The reaction was initiated by adsorption of NO_2 onto the zeolite in each case. In addition, the surface reactions were monitored using in situ FT-IR spectroscopy. Finally, quantitative relationships linking NO evolution to the number of ion-exchanged Fe sites were estimated using NO_2-TPD. The combination of mass balance analysis with in situ adsorbate detection allowed more complete elucidation of the NO evolution reaction.

2. Experimental

2.1. Catalyst preparation

A series of Fe/ZSM-5 catalysts was prepared by impregnation (Imp), reductive solid-state ion-exchange (RSIE), and CVD using varying Fe content [23]. As a starting zeolite, NH_4–ZSM-5 (Tosoh HSZ-830NHA, $Si/Al_2 = 28$, $S_{BET} = 350\ m^2\ g^{-1}$) was transformed to H–ZSM-5 by calcining at 873 K in air for 5 h.

For the Imp method, $Fe(NO_3)_3{\cdot}9H_2O$ (Wako, >99%) was added dropwise into a suspension of H-ZSM-5 at 353 K. The sample was then heated to 373 K to slowly evaporate any residual water, followed by a final drying step at 383 K to obtain the solid product. The dried sample was then calcined at 923 K in 20% O_2/N_2 for 5 h.

For the RSIE technique, Fe/ZSM-5 samples prepared using the Imp method were placed in a flow reactor, heated to 923 K at 5 K min^{-1} in a flowing 5% H_2/N_2, and maintained at the same temperature for 5 h. The sample was then calcined at 923 K in 20% O_2/N_2 for 5 h.

A more detailed procedure on how to use the CVD method was described previously by our laboratory [23]. Briefly, immediately following the calcining step at 923 K in N_2, dehydrated H-ZSM-5 was mixed mechanically in a glove box with an appropriate amount of $FeCl_3$ (Wako, >99%) for the desired Fe loading. The mixed dry powder was placed in a furnace, heated to 923 K at 5 K min^{-1}, and then maintained at the same temperature for 2.5 h under a flow of N_2 gas. The Fe-loaded sample was then washed twice with deionized water and dried at 383 K. The samples were then calcined at 923 K in 20% O_2/N_2 for 5 h. Finally, the samples were pelletized to grain sizes of 500–900 μm. Fe contents were determined using inductively coupled plasma (ICP) analysis, and the results are presented in Table 1.

2.2. NO_2 adsorption test and NO_2-TPD measurement

The NO_2 adsorption test and NO_2-TPD measurements were carried out under atmospheric pressure in a fixed-bed flow reactor (i.d. = 9 mm ∅) equipped with a quadrupole mass spectrometer (QMS, ULVAC messmate-200). A 400-mg sample was placed on a porous quartz plate. A predefined gas was then introduced through mass flow controllers. Prior to NO_2 adsorption, the samples were pretreated at 873 K for 30 min in a flow of 5% O_2/He (300 ml min^{-1}) and then cooled to 373 K, followed by switching to a He flow. The NO_2 adsorption test was carried out by introducing 0.45% NO_2/He (100 ml min^{-1}) at 373 K until complete saturation of adsorbed NO_2 had occurred (approximately 40 min). At this point, He (300 ml min^{-1}) was supplied at the same temperature for 30 min to help remove any extra nonadsorbed NO_2. The temperature of the samples was then lowered to 323 K, and NO_2-TPD measurements were carried out at a heating rate of 10 K min^{-1} from 323 to 873 K in a He flow of 100 ml min^{-1}.

The QMS analyses did not reveal any formation of N_2 or N_2O for either the NO_2 adsorption or NO_2-TPD tests. The NO_2 concentration was estimated from the intensity of the mass spectrometric signal at $m/e = 46$ (I_{46}). The NO concentration ([NO]) was calculated from I_{46} and the $m/e = 30$ signal intensity (I_{30}) according to

$$[NO] = I_{30} - c_1 \times c_2 \times I_{46} \quad (4)$$

This calculation was performed in order to eliminate the contribution of NO_2 fragmentation. Here, c_1 is the relative sensitivity of NO to NO_2 on I_{30}, and c_2 is the I_{30}/I_{46} fragmentation ratio for NO_2, which are both constant. In NO_2-TPD, the effluent gases were determined to be primarily NO_2 at lower temperatures (<623 K) and NO and O_2 at higher temperatures (>623 K), due to the $NO_2 \leftrightarrow NO + 1/2O_2$ equilibrium. From this, we determined the NO_x concentrations by combining the NO and NO_2 concentrations.

2.3. In situ FT-IR measurement

The FT-IR spectra were obtained using a diffuse reflectance accessory connected to an FT-IR spectrometer (Nicolet NEXUS 670) that was equipped with an MCT detector. The sample pellets were placed in an alumina cup (i.d. = 5 mm ∅, $d = 4$ mm) with many small holes on its bottom surface, allowing gas to flow uniformly through the sample bed from bottom (upstream relative to gas flow) to top (downstream relative to gas flow). A heating coil was installed just beneath the sample cup, allowing thermal treatment of the sample while gas was flowing. The total gas flow was maintained at 200 ml min^{-1} by mass flow controllers. An IR light was irradiated through a KBr window to the top layer of the sample.

Prior to the NO_2 adsorption test, the samples were pretreated in situ at 873 K in a flow of 5% O_2/N_2 for 20 min and then cooled to 373 K. The NO_2 adsorption was carried out at 373 K in a flow of 0.2% NO_2/N_2 for steady-state measurements and 0.1% NO_2/N_2 for time-resolved measurements. In the case of steady-state measurements performed at 323 K under N_2 flow, each spectrum was generated before and after NO_2 adsorption and involved the accumulation of 500 scans at a resolution of 4 cm^{-1}. For the time-resolved measurements with NO_2 flowing, each spectrum was generated following the accumulation of 30 scans taking approximately 12 s. All the spectra were then converted with the Kubelka–Munk (KM) function.

Table 1
Description of Fe/ZSM-5 and results of the NO_2 adsorption test (see Fig. 1) and NO_2-TPD test (see Fig. 7).

Catalyst	Fe content		NO_2 adsorption test		NO_2-TPD test	
	Fe/Al	wt.%	NO evolution[a]	Total NO_x adsorption[a]	HT peak[a]	Total NO_x desorption[a]
H-ZSM-5	–	–	2	217	19	148
Imp(0.25)[b]	0.25	1.53	3	252	34	178
Imp(0.5)[b]	0.50	3.00	7	247	41	182
Imp(1.0)[b]	1.00	5.75	4	248	48	195
Imp(1.5)[b]	1.50	8.28	10	253	50	195
RSIE(0.25)[c]	0.25	1.53	34	309	82	255
RSIE(0.5)[c]	0.50	3.00	51	323	96	257
RSIE(1.0)[c]	1.00	5.75	61	320	110	260
RSIE(1.5)[c]	1.50	8.28	64	299	110	246
CVD(0.29)[d]	0.29	1.76	45	308	92	224
CVD(0.44)[d]	0.44	2.67	58	308	116	234
CVD(0.61)[d]	0.61	3.62	69	290	118	213
CVD(0.78)[d]	0.78	4.55	76	331	126	248

[a] $\mu mol\ g^{-1}$.
[b] Prepared by impregnation method.
[c] Prepared by reductive solid-state ion-exchange method.
[d] Prepared by CVD method.

3. Results

3.1. NO evolution reaction following NO_2 introduction

It has already been reported that NO evolves immediately following the introduction of NO_2 to Fe/ZSM-5 in the presence of H_2O (1 vol.%) at 323–473 K [20,25]. Here, we describe NO evolution in the absence of H_2O using a series of Fe/ZSM-5 prepared with different methods and composed of varying Fe content. To investigate the NO evolution behavior of these samples, the NO_2 adsorption test was performed at 373 K. Shown in Fig. 1 are the outlet concentrations of NO and NO_2 measured as a function of time during the NO_2 evolution reactions carried out on H-ZSM-5 and on several Fe/ZSM-5 zeolites. For all samples tested, a release of NO was observed with the concomitant emission of NO_2 in the region of 200–600 s. (We also tested a blank run, though the NO evolution was not observed.) The peak shape of the NO evolution observed was broad and skewed for all samples. In addition, NO evolution was complete near the saturation point of NO_2. This observation, described in more detail in Section 3.2.2, indicates that the newly generated NO adsorbed temporarily onto the surface of the zeolites and then was ultimately replaced by follow-on NO_2.

The quantity of evolved NO varied greatly among the samples. For example, the amount of NO generated using CVD (0.61) (Fig. 1d), despite its lower Fe content, was much greater than that observed when Imp(1.5) was used (Fig. 1b). The amount of NO evolved and the total NO_x adsorbed for all samples tested are listed in Table 1. Close inspection of the data in Table 1 reveals that NO evolution is influenced more by the preparation method than by their absolute Fe content. This trend agrees well with the NH_3-SCR activity order of these catalysts [23], suggesting that the NO evolution reaction may depend on SCR active sites (discussed further in Section 4.1).

Grossale et al. [20,29] reported that NO_2 consumption and the concomitant NO evolution in the presence of H_2O may be explained by the formation of nitrates on the surface of the catalyst according to the following reaction:

$$3NO_2 + H_2O \leftrightarrow NO + 2HNO_3 \quad (5)$$

Grossale et al. [20,29] showed that the molar ratio of newly generated NO with respect to consumed NO_2 was approximately 1:3, which agrees with the stoichiometric values shown in reaction (5). Recently, Ahrens et al. [25] reported that this stoichiometry is preserved under an H_2O-free gas feed condition, although adsorbed water is present in Fe/zeolite.

In contrast to the proposals of the previous reports [20,25,29], our results indicate that the ratio of the evolved NO with respect to consumed NO_2, i.e., the sum of NO evolved and the total NO_x adsorbed (refer to Table 1), is more than 1:5 for all sample tested. When using H-ZSM-5, for instance, 219 $\mu mol\ g^{-1}$ of NO_2 was consumed, while the NO evolution was negligible (2 $\mu mol\ g^{-1}$). Additionally, a markedly different point between our data and the previous results is the timing of the breakthrough of NO; there are dead times (at least 200 s) for NO breakthrough after the introduction of NO_2 in our cases (see Fig. 1), while in the literature [20,25,29] NO leaked immediately after the NO_2 introduction. Given the fact that the dead times in Fig. 1 are nearly identical even though their NO_2 storage capacities are substantially different, the NO_2 adsorption would be composed of two general types: (a) weak NO_2 adsorption in the zeolite channel and (b) strong chemisorption to the Fe sites. Here, if we estimate the consumed NO_2 amounts from the breakthrough point, the ratios of evolved NO to consumed NO_2 become closer to 1:3. For example, the ratios are 1:3.0 for Imp(1.5) calculated after 290 s, 1:3.2 for RSIE(0.25) after 260 s, and 1:2.0 for CVD(0.61) after 200 s. Thus, the weakly adsorbed NO_2 must be one factor that shifts the ratios from the stoichiometry to higher values. In other words, we can say that the weakly adsorbed NO_2 is not related to the NO evolution reaction.

When it comes to NO adsorption to Fe/ZSM-5, on the other hand, Grossale et al. [20] mentioned that NO did not adsorb under H_2O present condition at 323–473 K, despite the fact that NO_2 was able to adsorb. In contrast, our findings suggest that NO also adsorb onto Fe/ZSM-5 at 353 K when using H_2O-free condition following pretreatment at high temperatures (see Fig. S1 in Supplementary material). Although the adsorption amount was lower than that for the NO_2 adsorption measurement, similar dead times before NO breakthrough were observed. This result implies that weak NO adsorption also occurred under this condition.

Thus, there is considerable discrepancy between the previous reports [20,29] and the results reported herein. The reason for these contradictions is likely due to the dehydration state of the zeolites. For example, because H_2O interacts strongly with the pores in zeolites, careful attention needs to be paid to the preparation methods used for generating dehydrated samples. Therefore, it is our assertion that complete dehydration of zeolite enables NO_2 to adsorb weakly in the zeolite channel. A similar conclusion has been reached by NO adsorption onto Cu/ZSM-5 [30] and Ag/MOR [31] and by NH_3 adsorption onto Fe/ZSM-5 [32].

For the experiments described herein, high-temperature treatment (873 K) under a high space velocity ($2.34 \times 10^4\ h^{-1}$) was

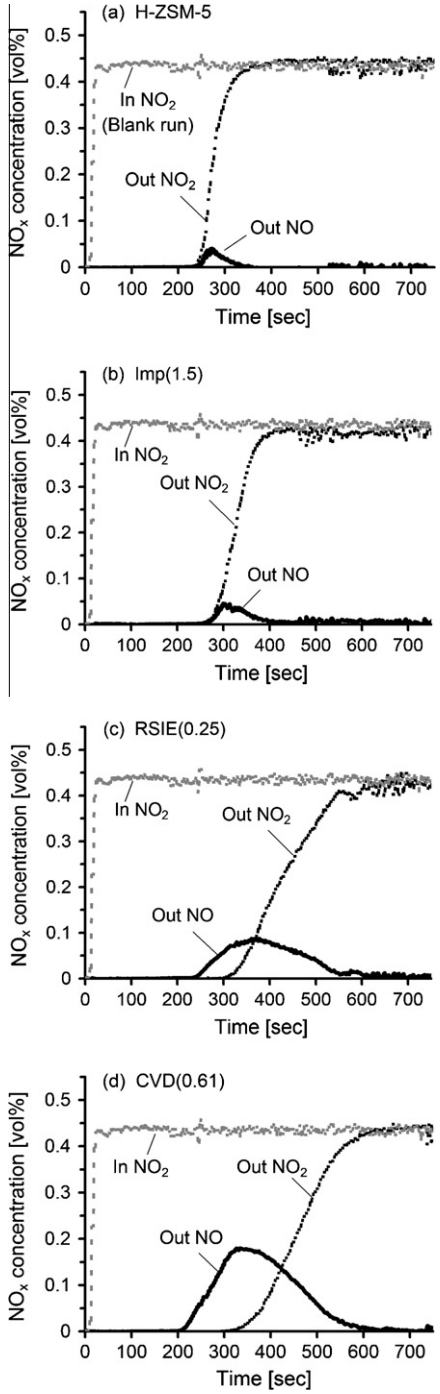

Fig. 1. Concentration profiles of NO and NO_2 using the NO_2 adsorption test over (a) H-ZSM-5 and Fe/ZSM-5 prepared by (b) Imp, (c) RSIE, and (d) CVD methods. Sample weight: 400 mg; pretreatment: 5% O_2/He (300 ml min^{-1}) at 873 K; measurement condition: 0.45% NO_2/He (100 ml min^{-1}) at 373 K.

performed prior to the NO_2 adsorption tests. Therefore, a direct reaction between NO_2 and H_2O such as reaction (5) is not expected following this pretreatment step due to insufficient levels of H_2O. If reaction (5) was favored, only the nitrate species would remain on the surface of the zeolite. However, FT-IR measurements (see Section 3.2.1) identified NO_2 as the most abundant product on the surface of the zeolites along with several other NO_x species, thus indicating that some adsorption reactions other than reaction (5) should progress when our pretreatment methods are used. Szanyi et al. [33] have investigated the effect of hydration on NO_2 adsorption states over Na–Y and Ba–Y zeolites by means of spectroscopic characterization. In the case of fully dehydrated zeolite, Szanyi et al. [33] reported that the NO_2 adsorption step proceeds via a NO_2 dimerization and disproportionation reaction:

$$2NO_2 \leftrightarrow N_2O_4 \leftrightarrow NO^+ + NO_3^- \quad (6)$$

Conversely, in the presence of H_2O, Szanyi et al. [33] reports that reaction (5) between NO_2 and H_2O occurs in addition to a reaction between NO^+ and H_2O. Taking the above-mentioned results into account, it is our expectation that in the case of our measurement, (a) weak NO_2 adsorption in the zeolite pore and (b) strong NO_2 adsorption that leads to NO evolution and/or disproportionation reaction (6) will be mixed. Detailed adsorption states and a detailed mechanism are discussed later in Sections 3.2 and 4.2, respectively.

3.2. In situ FT-IR measurement

3.2.1. Static measurement of NO_2 adsorption

To identify the adsorbed species, we first measured steady-state IR spectra before and after NO_2 adsorption. The NO_2 adsorption was performed at 373 K by flowing 0.2% NO_2/N_2 for 20 min. Spectra were recorded for this step at 323 K under a N_2 gas flow. Shown in Fig. 2 are the spectra for H-ZSM-5 and CVD(0.61).

Four bands were observed for H-ZSM-5 in the OH stretching region (3850–3450 cm^{-1}) (Fig. 2a). The bands seen at 3745, 3660, and 3610 cm^{-1} are assigned to terminal silanols, OH groups associated with extra-framework aluminum, and a bridging OH group (i.e., Brønsted acid sites), respectively [6,15,23,34,35]. The 3780-cm^{-1} band was assigned to an OH group attached to a tricoordinated aluminum atom in the zeolite framework [23,34,36]. This aluminum atom provides a coordinately unsaturated site, since some molecules are capable of adsorbing onto it, and thus results in a perturbation of the band [36]. Also seen in the case of H-ZSM-5 was a disappearance of the 3780 cm^{-1} band following NO_2 adsorption, indicating that NO_2 affected the hydroxyl group either directly or indirectly.

In the case of CVD(0.61), a new strong band at 3675 cm^{-1} was observed that was assigned to OH groups linked with ion-exchanged Fe (Fe–OH) [23,34,35,37]. The 3610 cm^{-1} band obtained on CVD(0.61) was smaller than that observed on H-ZSM-5 due to Fe ion-exchange on Brønsted sites. The decrease in Fe–OH band intensity following NO_2 adsorption likely occurs as a result of the OH groups on Fe becoming more disordered or replaced by NO_2.

Following pretreatments, a characteristic structure is observed in both H-ZSM-5 and CVD(0.61) spectra, in the NO_x stretching region (2300–1500 cm^{-1}) (dashed lines). These bands are assigned to overtones and combination bands involving zeolite framework vibration [15,38]. Three bands appeared for both samples following NO_2 adsorption (solid lines). The bands at 2140–2130, 1655–1635, and 1590–1570 cm^{-1} are assigned to NO^+ species, a NO_2 group and a nitrate group, respectively [13,22,23,35,39–41]. Due to the absence of any additional bands at 2250–2220, 1885–1860, and 1770–1740 cm^{-1}, the formation of N_2O, N_2O_3, and N_2O_4, respectively, may be ruled out [13,35,40,41]. Clearly, the absorption intensities of NO_2 and nitrate groups in CVD(0.61) were stronger than those observed for H-ZSM-5, which is in accordance with greater total NO_x adsorption on CVD(0.61) (see Fig. 1 and Table 1). Comparing each band position between the two samples, those associated with Fe/ZSM-5 were slightly lower than those observed for H-ZSM-5 ($\Delta\nu \approx 20\ cm^{-1}$), suggesting that the interaction strength between the adsorbate and the substrate is different.

In the zeolite framework vibration (T–O–T) region, only one band (820 cm^{-1}) was seen for H-ZSM-5, whereas an additional band at 915 cm^{-1} emerged with the CVD(0.61) sample. The band

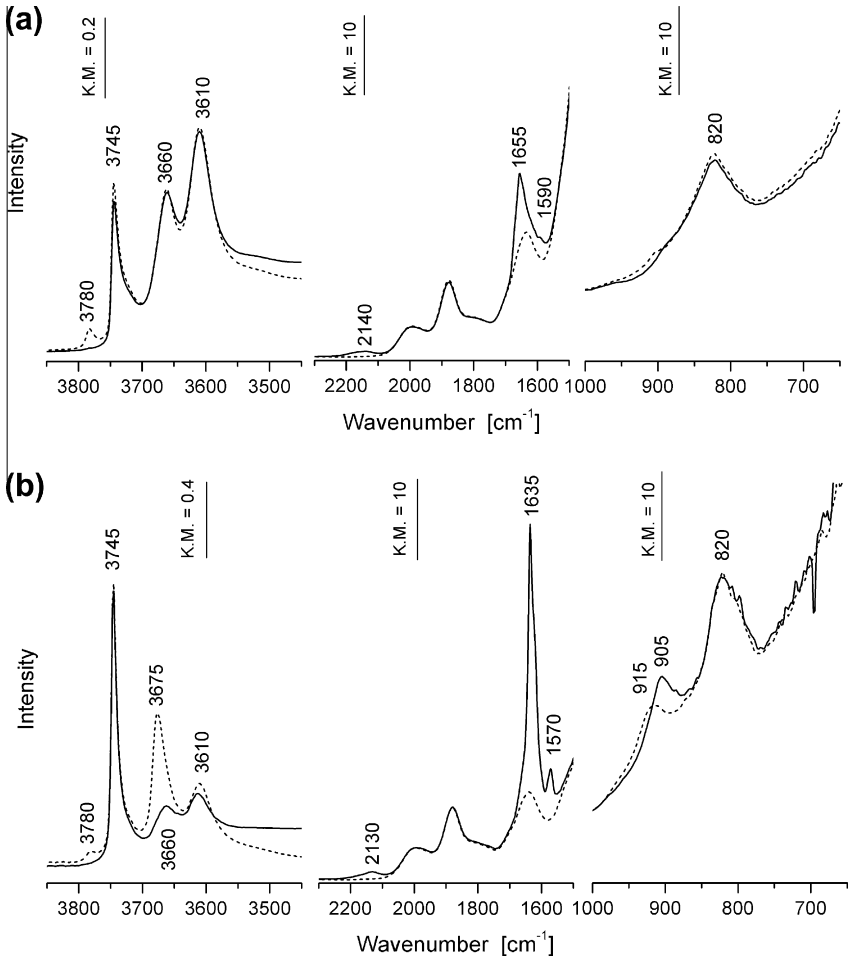

Fig. 2. Steady-state FT-IR spectra before (dashed lines) and after (solid lines) NO_2 adsorption over (a) H-ZSM-5 and (b) CVD(0.61). Pretreatment: 5% O_2/N_2 at 873 K; measurement: N_2 (200 ml min^{-1}) at 323 K.

at 820 cm^{-1} has been attributed to both internal and external symmetric T–O–T vibrations [22,23,40,42]. The band at 915 cm^{-1} is assigned to an internal asymmetric T–O–T vibration perturbed by ion-exchanged Fe^{3+} (unperturbed ring bands appear at 1130–1030 cm^{-1}) [22,23,40,42]. When NO_2 was introduced to CVD(0.61), the perturbed band shifted to a lower wavenumber; that is, from 915 to 905 cm^{-1} (Fig. 2b). This shift suggests that ion-exchanged Fe^{3+} interacts with NO_2 or with some other adsorbates derived from NO_2 [22,23]. This is consistent with the Fe–OH band (3675 cm^{-1}) decreasing in intensity following NO_2 adsorption. In contrast, the band at 820 cm^{-1} did not shift, which corroborates previous reports that this band is unaffected by either metal ion-exchange or molecular adsorption [22,23,40,42].

3.2.2. Transient time-resolved measurement of NO_2 adsorption

To track transient changes of the adsorption species, time-resolved measurement under 0.1% NO_2/N_2 flow was carried out at 373 K. Shown in Fig. 3 are the difference spectra within the NO_x stretching region for both H-ZSM-5 and CVD(0.61) samples. In the case of H-ZSM-5, three bands appeared that mimic ones observed in the static measurement (Fig. 2a). These bands increased rapidly when NO_2 was introduced. For CVD(0.61), however, a new band appeared at 1880 cm^{-1} (not observed in the static measurement) temporarily during the first stage of NO_2 adsorption, and then decreased in intensity with the concomitant saturation of the other three bands (2130, 1635, and 1570 cm^{-1}) (Fig. 2b). The new band at 1880 cm^{-1} was assigned to adsorbed NO species [35,39–41]. The observation of adsorbed NO agrees well with the NO evolution characteristics described in Section 3.1. That is, when results of the NO_2 adsorption test on H-ZSM-5 were compiled, the quantity of NO evolution was found to be negligible (Fig. 1a), and hence a NO peak was not observed (Fig. 3a). In the case of CVD(0.61), a greater amount of NO evolution was recorded (Fig. 1d) and temporal NO adsorption was also observed (Fig. 3b).

Fig. 4a shows the difference spectra in the region 3900–2500 cm^{-1} acquired for CVD(0.61) at seven representative points. The assignments of the three OH bands (3745, 3675, and 3610 cm^{-1}) are the same as those observed in Fig. 2b. The band at 3245 cm^{-1} is assigned to the first overtone band of 1635 cm^{-1} (see Fig. 2b), and that at 2605 cm^{-1} is assigned to a combination mode of 1635 cm^{-1}, with another mode (undetectable) at ca. 970 cm^{-1} [22,43,44]. The intensity profiles of the four bands (3675, 3610, 3245, and 2605 cm^{-1}) are presented in Fig. S2 in Supplementary material. The bands at 3675 cm^{-1} (Fe–OH) and at 3610 cm^{-1} (Brønsted acid OH) decreased rapidly following the introduction of NO_2. Meanwhile, the bands at 3245 and 2605 cm^{-1} (NO_2 related bands) began to increase at ca. 12 min. This time-lag stems from differences in the corresponding adsorption species, as is discussed below.

Fig. 4b shows the difference spectra in the NO_x stretching region, and Fig. S3 in Supplementary material shows peak intensity profiles of the four bands observed in Fig. 4b. Close inspection of the spectra in Fig. 4b reveals that the bands at 1880 and 1635 cm^{-1} may each be composed of two or more peaks, suggesting that there may possibly

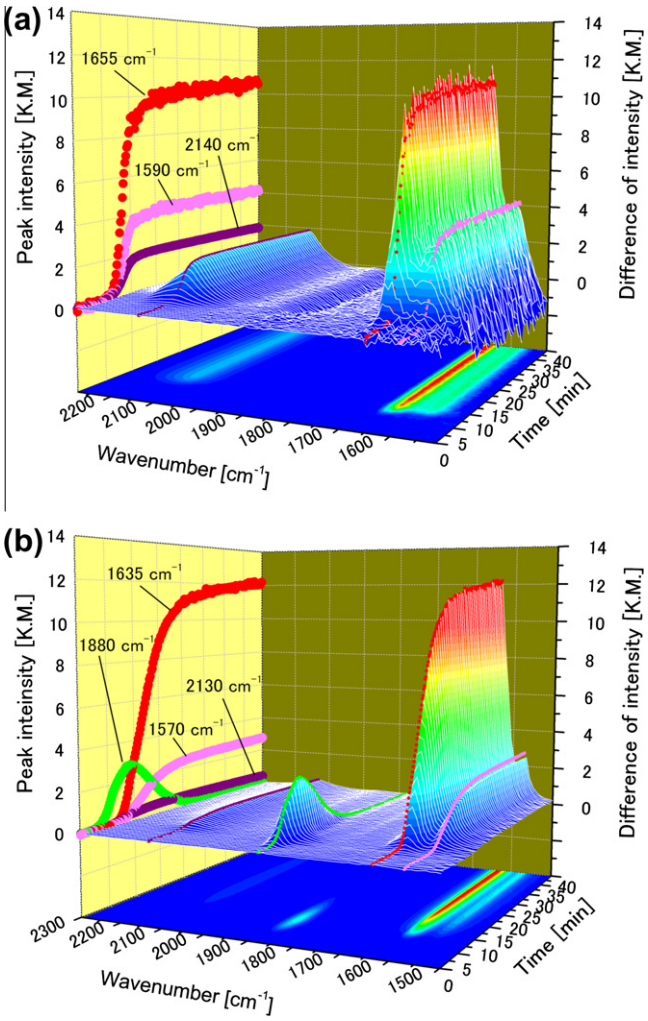

Fig. 3. Time-resolved difference FT-IR spectra during NO_2 adsorption over (a) H-ZSM-5 and (b) CVD(0.61). Measurement condition: 0.1% NO_2/N_2 (200 ml min^{-1}) was introduced from N_2 flow in 2 min at 373 K.

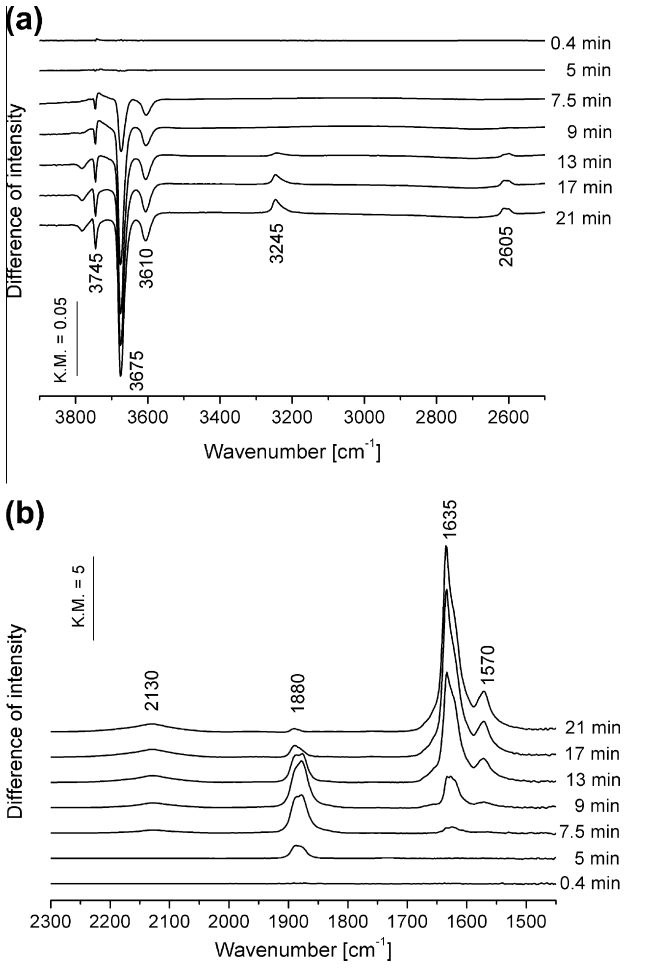

Fig. 4. Difference FT-IR spectra before and after NO_2 adsorption of CVD(0.61) at seven representative points along the timed-resolved measurement (a) in the 3900–2500 cm^{-1} and (b) in the 2300–1400 cm^{-1} region. Conditions are the same as those reported for Fig. 3.

be other species with slightly different chemical states [35], or some dipole–dipole coupling between adsorbed molecules [45]. In general, however, the band at 1880 cm^{-1} (NO) appeared first, followed by the bands for NO_2 and nitrate at 1635 and 1570 cm^{-1}, respectively. The 1880-cm^{-1} band intensity reached a maximum at ca. 9.5 min and then decreased with a concomitant increase in the band intensities at 1635 and 1570 cm^{-1}. After that, the band at 1880 cm^{-1} disappeared when the signals for the other species were near saturation.

To examine the relationships between the band intensity profiles in Fig. 4a and b, each band intensity was normalized at the maximum or minimum intensity in the profiles. Fig. 5a shows normalized profiles of bands at 2130 cm^{-1} (NO^+) and 3610 cm^{-1} (Brønsted OH) that appear to be mirror images of each other, thus indicating that NO^+ adsorbed selectively onto the sites; that is, Brønsted H^+ was replaced by NO^+:

$$Zeo^-O{-}H^+ + NO^+ \leftrightarrow Zeo^-O{-}NO^+ + H^+ \quad (7)$$

However, the absolute intensities of both bands were small (see Fig. 4a and b) such that these species and the reaction (7) may be considered as negligible when comparing to all other NO_x adsorbates and their corresponding reactions.

Interestingly, the band at 2130 cm^{-1} decreased gradually with a concomitant increase in the band at 3610 cm^{-1} after 20 min. One reasonable explanation for this observation is that NO^+ may react with negatively charged species at the surface, such as oxygen atoms, leading to the formation of nitrite groups (NO_2^-) that correspond to signals near 1350 cm^{-1} [22,41,46]. However, signals originating from nitrite groups were not easily detected due to interfering background signal caused by zeolite lattice vibration. Hence, improving signal-to-noise in this region of the spectrum would require that measurements be taken at low temperatures.

Normalized profiles of bands at 3675 cm^{-1} (Fe–OH), 1880 cm^{-1} (NO), 1635 cm^{-1} (NO_2), and 1570 cm^{-1} (nitrate) are shown in Fig. 5b. A maximum point at 1880 cm^{-1} (ca. 9.5 min) is generally consistent with an ending point having a sharp decline at 3675 cm^{-1}, suggesting that the decrease in Fe–OH is strongly related to NO adsorption on the Fe sites. At approximately that time, the bands at 1635 and 1570 cm^{-1} began to increase in intensity. The increasing profiles of bands at 1635 and 1570 cm^{-1} and the decreasing profile of the band at 1880 cm^{-1} occurred in a symmetric fashion, thus indicating that adsorbed NO was replaced by NO_2. The assignments of the bands at 1635 and 1570 cm^{-1} are discussed in more detail in Section 4.2.

A limitation of the FT-IR measurements described in Section 2.3 is the inability to distinguish NO originally formed at the bottom of the sample (upstream) versus that formed at the top of the sample (on site). Since our experiments were designed to be set up as an integral reactor, and all measurements arise solely from the top

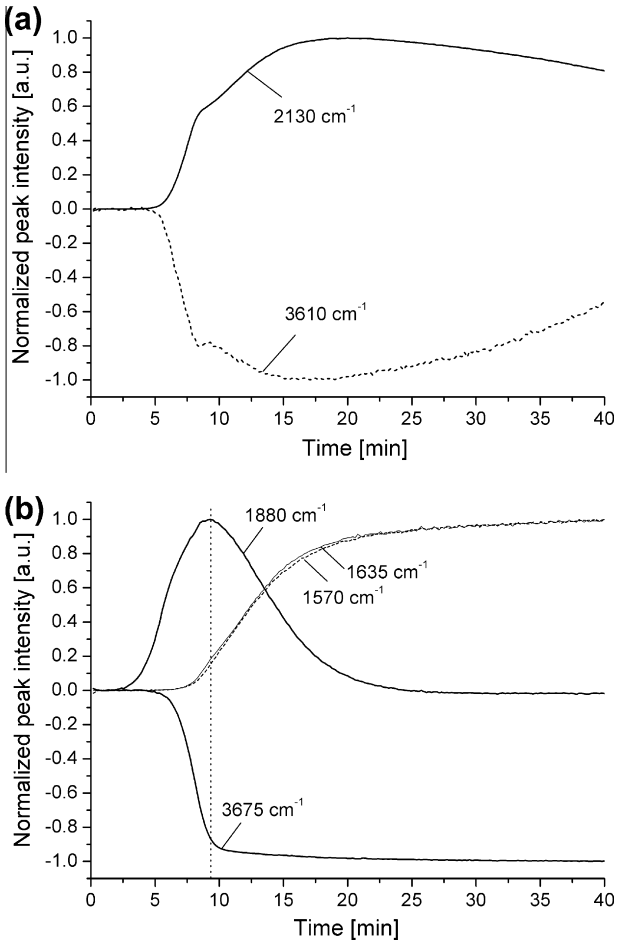

Fig. 5. Normalized peak intensity profiles associated with the bands in Fig. 4. (a) Comparison of the bands at 2130 and 3610 cm^{-1} and (b) comparison of the bands at 3675, 1880, 1635, and 1570 cm^{-1}. Normalization was conducted at the maximum or minimum intensity point to each band.

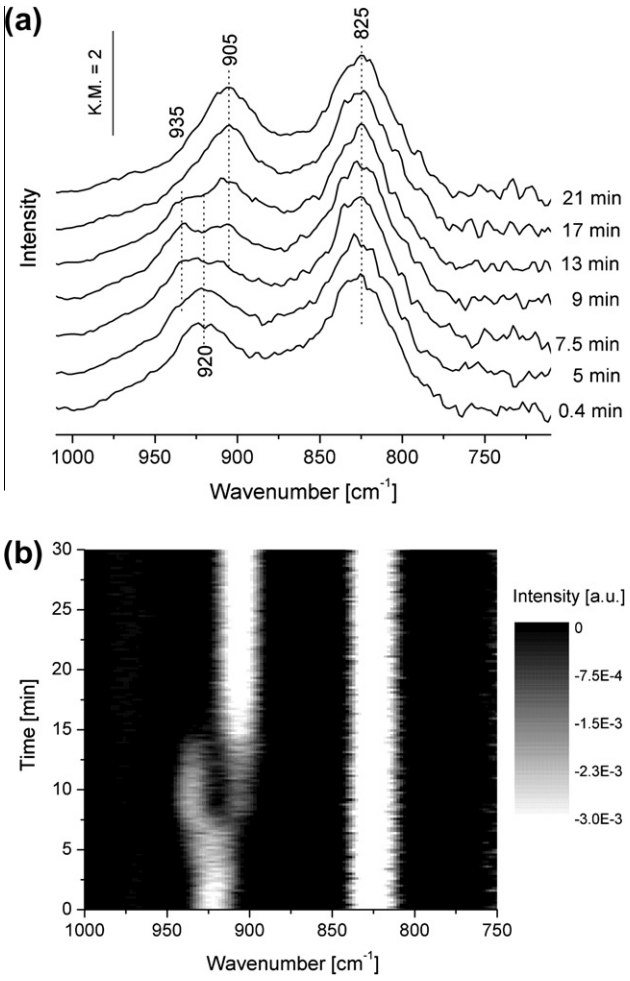

Fig. 6. (a) T–O–T region spectra of CVD(0.61) after subtraction of background at seven representative points on time-resolved measurement. (b) Second derivatives of time-resolved spectra after application of a background subtraction and smoothing operation.

of the sample, we hypothesize that the majority of measured NO originates from the bottom of the sample, and then migrates upward (downstream) within the sample. Avoiding this limitation would require the use of a differential reactor combined with higher time-resolved analyses [47,48].

Fig. 6a shows the difference spectra in the T–O–T region. The band at 825 cm^{-1} remained unchanged during supply of NO_2, whereas the perturbed band at 920 cm^{-1} was split into lower and higher bands (ca. 9 min): an increasing red-shifted band at 905 cm^{-1} and a decreasing blue-shifted band at 935 cm^{-1}. It has been reported that the position of the perturbed band is dependent upon the Fe oxidation state and/or on molecular adsorption [22,23,40,42].

To characterize the perturbation behavior in more detail, we conducted a smoothing operation and then differentiated the spectra at two separate times. This second-derivative analysis is often applied to a minute investigation of spectrum peaks [35]. Fig. 6b shows the result of mapping the second-derivative spectra against time. First, at 4–7 min, the perturbed band shifted slightly to a higher wavenumber. Then, a strong blue-shifted band and a weak red-shifted band appeared (ca. 8 min). This was followed by an increase in the red-shifted band and a concomitant decrease in the blue-shifted band (8–14 min).

The blue-shifted band (935 cm^{-1}) is caused by adsorbed NO as determined from its time range (5–15 min), and the strongest point (ca. 10 min) agrees with the intensity profile of the adsorbed NO band (1880 cm^{-1}) in Fig. 5b. The red-shifted band (905 cm^{-1}) appeared at approximately 8 min and increased sharply up to 15 min (Fig. 6a and b), agreeing with the behavior of the adsorbed NO_2 (1635 cm^{-1}) and nitrate (1570 cm^{-1}) bands in Fig. 5b.

As for the blue-shift of the perturbed T–O–T band, Gao et al. [40] and Mauvezin et al. [42] observed that the band shifts to a higher wavenumber when the preoxidized Fe/ZSM-5 is reduced. Also, Gao et al. [40] investigated changes in the perturbed band following NO adsorption on preoxide samples. Close inspection of the spectra presented by Gao et al. [40] indicates that the band position under NO adsorption is blue-shifted when compared to the preoxide state. Additionally, it has been reported that Fe^{3+}–OH species are reduced by NO, even at low temperature, over Fe/ZSM-5 [35], Fe/BEA [49], and Fe/FER [50] by FT-IR analysis. Xia et al. [14] recently proposed NO treatment over Fe/ZSM-5 can remove hydroxyl groups bound to the binuclear Fe^{3+} sites leading to the formation of binuclear Fe^{2+} sites. In summary, these findings suggest that the Fe electronic state or the surrounding bonding state is modified by the interaction of Fe with NO, which causes the blue-shift of the perturbed band.

As for the red shift of the perturbed T–O–T band, Gao et al. [40] investigated changes in the band following $NO + O_2$ adsorption. Their spectra show that the band position under $NO + O_2$ adsorption is slightly red-shifted when compared to the preoxide state. Furthermore, we have previously reported that the perturbation

band shifts to a lower wavenumber (red shift) due to NO_2 adsorption and hypothesized that the oxidation state and/or coordination state of Fe should be changed compared to the preoxidized state [22,23]. A similar conclusion was reached using EXAFS studies of an N_2O adsorption system [51,52], where measurement of the Fe–O bond length is suggestive of a higher Fe oxidation state following N_2O treatment ($Fe^{(3+\delta)+}$) than is the case following O_2 treatment (Fe^{3+}).

3.3. NO_2-TPD

NO_2-TPD was carried out following the NO_2 adsorption test described in Section 3.1. Fig. 7 shows the NO_2-TPD spectra of several samples. We have previously reported that the TPD spectra of Fe/ZSM-5 have two distinct peaks [23]: a low-temperature (LT) peak that is essentially independent of Fe content (Fig. 7) and a high-temperature (HT) peak that is strongly affected by the preparation methods (i.e., Fe ion-exchange efficiency) according to the following : CVD > RSIE > Imp [23]. The LT peak has been assigned to weakly adsorbed NO_x in the zeolite channel, and the HT peak to chemisorbed NO_x bonded to ion-exchanged Fe sites [23].

The amounts of NO_x desorption are listed in Table 1 and are relative to both the HT peak and the total NO_x desorption for the complete range of temperatures. Interestingly, the total NO_x desorption amount using NO_2-TPD is lower than the total adsorption amount for each sample tested. This observation is likely due to the contribution of reversible adsorption of NO_2. From Table 1, the reversible adsorption rate of NO_2, under 0.45% NO_2/N_2 partial pressure, accounted for 17–32% of the total adsorption amount. For example, Despres et al. [24] quantified both adsorption and desorption of NO_2 on Cu/ZSM-5 at 473 K, resulting in 165 μmol g^{-1} of total adsorption versus only 116 μmol g^{-1} of total desorption measured by TPD, suggesting that approximately 30% reversible adsorption had occurred. For the samples tested in our studies, a wide range of reversible adsorption rates were measured owing to the use of different preparation methods and varying Fe contents [23], ultimately leading to the incorporation of varying amounts of Fe_xO_y small particles that inevitably affect zeolite micropore distribution.

4. Discussion

4.1. Relationships between NO evolution and HT peak

Shown in Fig. 8 is a plot of the amount of NO evolution versus the HT peak from the NO_2-TPD test. The NO evolution amount has a strong correlation with the HT peak, suggesting that the NO evolution occurs on the ion-exchanged Fe sites. This agrees well with the FT-IR results in Section 3.2. However, the Imp samples had certain amounts of HT peak despite having negligible amounts of NO evolution, while elevated levels of NO evolution and a large HT peak were observed for the RSIE and CVD samples. This implies that some specific structure among the ion-exchanged Fe sites should be active and should be formed only within a high-Fe-exchange region. We hypothesize such a region to be oligomeric structures on the ion-exchange sites, including an Fe binuclear structure, since it has already been reported that these species are formed when the Fe exchange rate exceeds a certain threshold, while isolate species mainly dominate in low-exchange regions [8,52,53]. In fact, the degrees of ion-exchange for the Imp samples are significantly lower than those for the RSIE and CVD samples (the major species in the Imp samples is the Fe_2O_3 particle outside of the zeolite pore) [23].

To obtain a more quantitative analysis, we calculated the ratio of the amount of NO evolution to the HT peak amount (Fig. 9). For the RSIE and CVD samples, all ratios fall within the range 0.4–0.6. If we assume that essentially all exchanged sites are binuclear, and since the HT peak has been assigned to the number of exchanged Fe sites, it may be expected that one NO molecule evolves from one binuclear site. The slight rise in ratio with increasing HT peak may be due to the contributions from minor species; that is, the existence of monomer on the side in smaller amounts and of trimer on the side in larger amounts.

4.2. Active site and NO evolution mechanism

In the previous section, we inferred that NO evolution occurred at the oligomeric structures on the ion-exchanged sites, such as binuclear Fe. Several researchers have insisted that binuclear Fe should be the active species for N_2O decomposition [14,17,19] or HC oxidation [8–10]. In addition, highly reactive oxygen on the binuclear site has been a contentious topic for some reactions studied to date [11,12,37,52]. For this reason, several studies have been performed to understand how highly reactive oxygen is generated and its role in these reactions. Nobukawa et al. [8,34,52] studied the N_2O reduction reaction with CH_4, using several characterization techniques. They reported that the binuclear Fe sites have a vacancy site between two Fe ions and that the active "nascent oxygen" atom ($O^*(a)$) may be generated at this site following N_2O dissociation. The existence of vacancy sites has been also proposed by

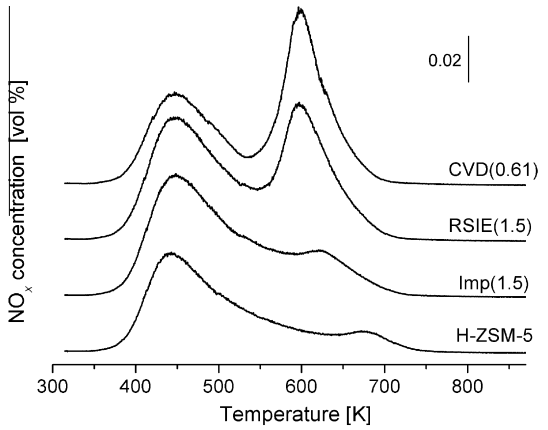

Fig. 7. NO_2-TPD spectra of H-ZSM-5 and several Fe/ZSM-5. Sample weight: 400 mg, flow rate: 100 ml min^{-1}, heating rate: 10 K min^{-1}.

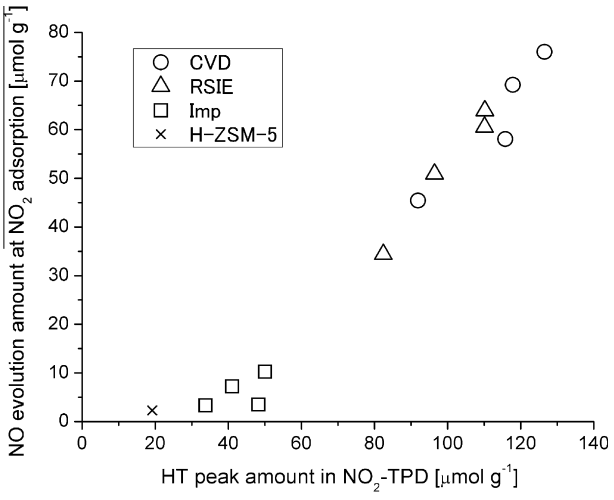

Fig. 8. Relationship between the NO evolution amount from the NO_2 adsorption test (see Fig. 1) and the HT peak amount associated with the NO_2-TPD test (see Fig. 7).

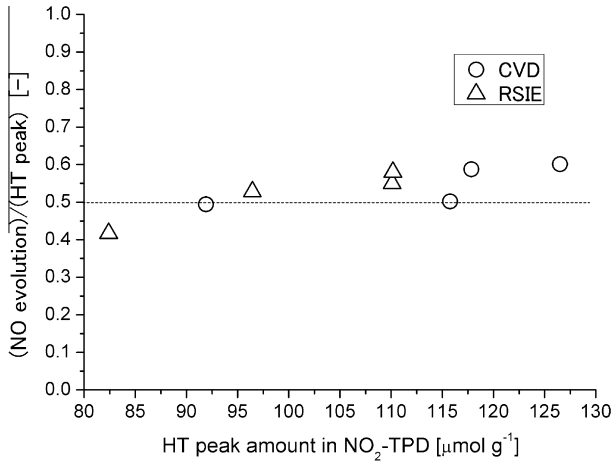

Fig. 9. Relationship between the ratio of NO evolution to HT peak and the HT peak amount.

other groups [54]. Nobukawa et al. [52] claim nascent oxygen plays an important role in activating CH_4, yet has a short lifetime and is converted rapidly to inactive species, such as the "accommodated oxygen" atom (O(a)).

In summary, we propose a NO evolution process as presented in Scheme 1a. First, the Fe–OH species and bridging vacancy sites are available following pretreatment. The former statement was confirmed by FT-IR spectra (Fig. 2b), while the latter one was speculated on after EXAFS analysis [8,52,54]. Second, when NO_2 is introduced, NO and bridging oxygen are produced from the decomposition of NO_2, and then NO is temporarily adsorbed onto the Fe sites. Third, adsorbed NO is then evolved with accompanying substitution of follow-on NO_2.

Scheme 1a is definitely the key scheme to describe the NO evolution reaction on the Fe sites, although it should practically take place only at an upstream position in the catalyst bed. As for the downstream position where in situ FT-IR monitored, on the other hand, Scheme 1b would mainly progress. First, NO generated originally at the upstream position flows into the downstream and then adsorbs onto the Fe sites. This can be explained by the appearance of NO bands with the concomitant disappearance of the Fe–OH band (Fig. 5b) as well as an observed shift of the perturbed T–O–T band to higher wavenumber (Fig. 6b). Second, follow-on NO_2 is replaced with adsorbed NO and decomposes to produce bridging oxygen with the same step as Scheme 1a. This was inferred from the symmetric fashion of NO and NO_2 profiles (a) on the NO_x outlet concentrations (Fig. 1d); (b) on the NO_x stretching bands (Fig. 5b); and (c) on the perturbed T–O–T bands (Fig. 6b).

This exchange reaction between NO and NO_2 implies that the adsorption equilibrium constant for NO_2 is larger than that for NO, as supported by previous SCR kinetic studies performed in our laboratory under fast SCR conditions [21]. Furthermore, previous NO_2-TPD kinetic studies performed in our laboratory measured the desorption energy of NO_2 from Fe sites at 138 kJ/mol [22], a relatively large value comparable to that measured for NH_3.

Overall, Scheme 1 shows that three NO_2 molecules are consumed to produce one NO molecule. This ratio agrees well with the results in the presence of H_2O [20,25,29]. Also, Scheme 1 states that the ratio of NO evolution to NO_2 adsorption on the Fe sites is 0.5, which is supported by the results reported in Fig. 9, where ratios of NO evolution to HT peak intensity were nearly 0.5. The same stoichiometry was observed on different materials such as Cu/ZSM-5 [24] and BaO/Al_2O_3 [26,27]. Considering the general chemistry of NO_2 adsorption, we believe that it is essential for active species to possess not only the NO_2 decomposition ability but also a property that can accommodate the atomic oxygen generated, such as Fe–□–Fe as in the case of Fe/zeolite. For Cu/ZSM-5, Despres et al. [24] explained the mechanism by assuming Cu dimer species. In the case of BaO/Al_2O_3, Nova et al. [26] mentioned the formation of Ba peroxide ($BaO–NO_2 \rightarrow BaO_2 + NO$) as an intermediate step in reaction (3).

On the possibility of N_2O_4 formation, although it was not detected in our experiments, we cannot rule out NO_2 dimerization during the adsorption process for the following reasons: First, under room-temperature or lower-temperature conditions, adsorbed N_2O_4 over Fe/ZSM-5 has been observed in several studies [13,35,40,41]. Second, in many oxide systems, including zeolites, NO_2 adsorption is considered to proceed via dimerization and disproportionation reactions (7) [13,22,46,55,56]. Third, NO_2 desorption from Fe/ZSM-5 is a second-order process, suggesting that the reverse reaction of NO_2 dimerization or other types of NO_2–NO_2 interaction participate in the overall desorption process [22]. In summary, it is reasonable to assume that dimerization of NO_2 may proceed through unstable N_2O_4, which is undetectable due to its very short lifetime.

During NO_2 adsorption, the principal NO_x adsorbates observed were the NO_2 group (1635 cm^{-1}) and nitrate species (1570 cm^{-1}) (Fig. 4b). However, normalized intensity profiles for both bands were completely consistent with each other (Fig. 5b). A similar observation has been reported by Poignant et al. [44] for Cu/ZSM-5 under $NO + O_2$, where a good correlation was found between bands at 1625 and 1565 cm^{-1} with varying NO_x partial pressure. As such, Poignant et al. [44] concluded that these bands arise from only one species. From this, we assume that the bands at 1635 and 1570 cm^{-1} may also be strongly related to each other. If this is the case, we can expect that NO_2 and nitrate are in an equilibrium state via bridging oxygen, as described in Scheme 2.

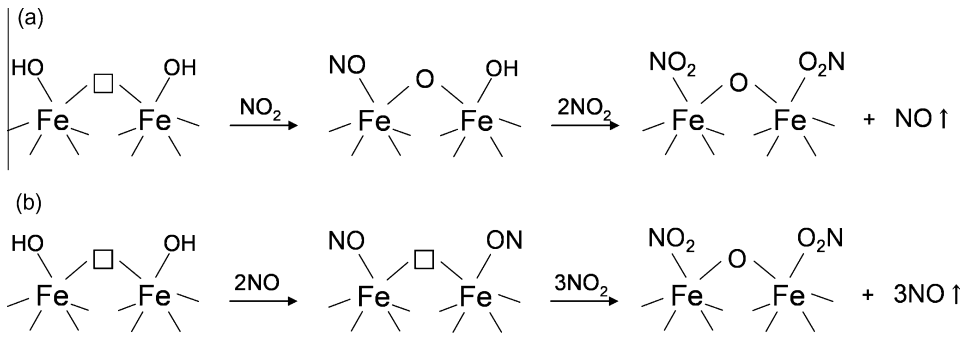

Scheme 1. Representation of the NO evolution mechanism with NO_2 adsorption over the Fe sites at (a) upstream and (b) downstream positions in the catalyst bed.

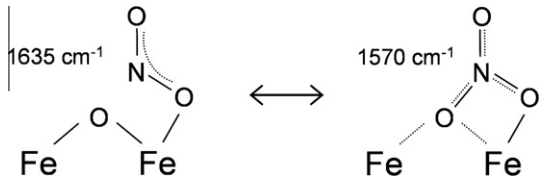

Scheme 2. Proposed equilibrium state of NO_2 adsorption on the Fe binuclear site.

However, further verification into the validity of Scheme 2 would require more rigorous IR studies using, for example, isotopic labeling [57], pulse response analyses [47,58], equilibrium pressure dependence [9,13,35], or higher-resolution IR techniques [48].

5. Conclusions

The NO evolution reaction following NO_2 introduction was investigated using a series of Fe/ZSM-5 catalysts prepared using different methods and composed of varying Fe content. NO evolution amounts from H-ZSM-5 and Fe/ZSM-5 prepared by the Imp method were very low, whereas a greater amount of NO evolution was observed using Fe/ZSM-5 prepared by the RSIE and CVD methods. This indicated that NO evolution is strongly correlated to the ion-exchanged Fe sites. Thus, we tracked the reaction by means of in situ FT-IR spectroscopy. Time-resolved measurement suggested that NO was created on the ion-exchanged Fe site. The newly generated NO was temporarily adsorbed onto the zeolites and then desorbed with accompanying substitution by follow-on NO_2. Comparison with HT peak intensities on NO_2-TPD, which are related to the amounts of ion-exchanged Fe, indicated that NO evolution was strongly correlated with the HT peak intensities. In the RSIE and CVD samples, the amount of NO evolution was nearly half as much as that associated with the HT peaks. From this, it may be concluded that one NO molecule evolves from one binuclear site, provided that the majority of the exchanged Fe on the RSIE and CVD samples are binuclear. Accordingly, the NO evolution mechanism may be described as follows: NO_2 is decomposed into NO and atomic oxygen over the Fe sites, which are probably oligomeric structures, including the Fe binuclear; decomposed oxygen occupies vacancy sites between Fe ions and acts as a chemical bridge; newly generated NO becomes temporally adsorbed onto the Fe site followed by its replacement with NO_2. In summary, this study demonstrates a general picture of an NO evolution mechanism by NO_2 introduction over Fe-loaded zeolites and provides a more detailed physicochemical understanding of the nature of ion-exchanged Fe sites, which are vital components of many reactions on Fe-zeolite catalysts.

Acknowledgment

We thank Kiyoshi Yamazaki and Banno Koji in Toyota Central R&D Laboratories for their helpful instructions.

Appendix A. Supplementary material

Supplementary data associated with this article can be found, in the online version, at doi:10.1016/j.jcat.2010.04.023.

References

[1] R.Q. Long, R.T. Yang, J. Am. Chem. Soc. 121 (1999) 5595.
[2] A.-Z. Ma, W. Grünert, Chem. Commun. (1999) 71.
[3] M. Schwidder, M.S. Kumar, K. Klementiev, M.M. Pohl, A. Brückner, W. Grünert, J. Catal. 231 (2005) 314.
[4] X. Feng, W.K. Hall, Catal. Lett. 41 (1996) 45.
[5] M. Schwidder, S. Heikens, A.D. Toni, S. Geisler, M. Berndt, A. Brückner, W. Grünert, J. Catal. 259 (2008) 96–103.
[6] A. Ribera, I.W.C.E. Arends, S. de Vries, J. Pérez-Ramírez, R.A. Sheldon, J. Catal. 195 (2000) 287.
[7] E.J.M. Hensen, Q. Zhu, R.A. van Santen, J. Catal. 220 (2003) 260.
[8] T. Nobukawa, M. Yoshida, K. Okumura, K. Tomishige, K. Kunimori, J. Catal. 229 (2005) 374.
[9] J. Long, W. Wang, Z. Ding, Z. Zhang, H. Lin, W. Dai, X. Fu, J. Catal. 264 (2009) 163.
[10] H. Xia, K. Sun, K. Sun, Z. Feng, W.X. Li, C. Li, J. Phys. Chem. C 112 (2008) 9001.
[11] K.A. Dubkov, N.S. Ovanesyan, A.A. Shteinman, E.V. Starokon, G.I. Panov, J. Catal. 207 (2002) 341.
[12] G.D. Pringruber, P.K. Roy, R. Prins, J. Catal. 246 (2007) 147.
[13] M. Rivallan, G. Ricchiardi, S. Bordiga, A. Zecchina, J. Catal. 264 (2009) 104.
[14] H. Xia, K. Sun, Z. Liu, Z. Feng, P. Ying, C. Li, J. Catal. 270 (2010) 103.
[15] P. Marturano, L. Drozdová, A. Kogelbauer, R. Prins, J. Catal. 192 (2000) 236.
[16] A.A. Battiston, J.H. Bitter, F.M.F. de Groot, A.R. Overweg, O. Stephan, J.A. van Bokhoven, P.J. Kooyman, C. van der Spek, G. Vankó, D.C. Koningsberger, J. Catal. 213 (2003) 251.
[17] N. Hansen, A. Heyden, A.T. Bell, F.J. Keil, J. Catal. 248 (2007) 213.
[18] J. Li, S. Li, J. Phys. Chem. C 112 (2008) 16938.
[19] H. Guesmi, D. Berthomieu, L. Kiwi-Minsker, J. Phys. Chem. C 112 (2008) 20319.
[20] A. Grossale, I. Nova, E. Tronconi, Catal. Today 136 (2008) 18.
[21] M. Iwasaki, K. Yamazaki, H. Shinjoh, Appl. Catal. A: Gen. 366 (2009) 84.
[22] M. Iwasaki, H. Shinjoh, Phys. Chem. Chem. Phys. 12 (2010) 2365.
[23] M. Iwasaki, K. Yamazaki, K. Banno, H. Shinjoh, J. Catal. 260 (2008) 205.
[24] J. Despres, M. Koebel, O. Kröcher, M. Elsener, A. Wokaun, Microporous Mesoporous Mater. 58 (2003) 175.
[25] M. Ahrens, O. Marie, P. Bazin, M. Daturi, J. Catal. 271 (2010) 1.
[26] I. Nova, L. Castoldi, L. Lietti, E. Tronconi, P. Forzatti, F. Prinetto, G. Ghiotti, J. Catal. 222 (2004) 377.
[27] N.W. Cant, I.O.Y. Liu, M.J. Patterson, Appl. Catal. B: Environ. 77 (2007) 12.
[28] I. Atribak, B. Azambre, A.B. López, A. García-García, Appl. Catal. B: Environ. 92 (2009) 126.
[29] A. Grossale, I. Nova, E. Tronconi, J. Catal. 265 (2009) 141.
[30] W.-X. Zhang, H. Yahiro, N. Mizuno, J. Izumi, M. Iwamoto, Langmuir 9 (1993) 2337.
[31] W. Zhang, M. Jia, J. Yu, T. Wu, Chem. Mater. 11 (1999) 920.
[32] N. Katada, T. Miyamoto, H.A. Begum, N. Naito, M. Niwa, A. Matsumoto, K. Tsutsumi, J. Phys. Chem. B 104 (2000) 5511.
[33] J. Szanyi, J.H. Kwak, S. Burton, J.A. Rodriguez, C.H.F. Peden, J. Electron Spectrosc. Relat. Phenom. 150 (2006) 164.
[34] S. Kameoka, T. Nobukawa, S. Tanaka, S. Ito, K. Tomishige, K. Kunimori, Phys. Chem. Chem. Phys. 5 (2003) 3328.
[35] M. Mihaylov, E. Ivanova, N. Drenchev, K. Hadjiivanov, J. Phys. Chem. C 114 (2010) 1004.
[36] A. Vimont, F. Thibault-Starzyk, J.C. Lavalley, J. Phys. Chem. B 104 (2000) 286.
[37] G.I. Panov, E.V. Starokon, L.V. Pirutko, E.A. Paukshtis, V.N. Parmon, J. Catal. 254 (2008) 110.
[38] A. Zecchina, S. Bordiga, G. Spoto, D. Scarano, G. Petrini, G. Leofanti, M. Padovan, C.O. Areàn, J. Chem. Soc. Faraday Trans. 88 (1992) 2959.
[39] R.Q. Long, R.T. Yang, J. Catal. 207 (2002) 224.
[40] Z.-X. Gao, Q. Sun, W.M.H. Sachtler, Appl. Catal. B: Environ. 33 (2001) 9.
[41] Q. Sun, Z.-X. Gao, H.-Y. Chen, W.M.H. Sachtler, J. Catal. 201 (2001) 89.
[42] M. Mauvezin, G. Delahay, B. Coq, S. Kieger, J.C. Jumas, J. Olivier-Fourcade, J. Phys. Chem. B 105 (2001) 928.
[43] K. Hadjiivanov, Catal. Lett. 68 (2000) 157.
[44] F. Poignant, J.L. Freysz, M. Daturi, J. Saussey, Catal. Today 70 (2001) 197.
[45] C. Tang, S. Zou, M.W. Severson, M.J. Weaver, J. Phys. Chem. B 102 (1998) 8546.
[46] C. Sedlmair, B. Gil, K. Seshan, A. Jentys, J.A. Lercher, Phys. Chem. Chem. Phys. 5 (2003) 1897.
[47] A. Wille, E. Fridell, Appl. Catal. B: Environ. 70 (2007) 294.
[48] F. Thibault-Starzyk, E. Seguin, S. Thomas, M. Daturi, H. Arnolds, D.A. King, Science 324 (2009) 1048.
[49] R. Kefirov, E. Ivanova, K. Hadjiivanov, S. Dzwigaj, M. Che, Catal. Lett. 125 (2008) 209.
[50] V. Blasin-Aubé, O. Marie, J. Saussey, A. Plesniar, M. Daturi, N. Nguyen, C. Hamon, M. Mihaylov, E. Ivanova, K. Hadjiivanov, J. Phys. Chem. C 113 (2009) 8387.
[51] J. Jia, Q. Sun, B. Wen, L.X. Chen, W.M.H. Sachtler, Catal. Lett. 82 (2002) 7.
[52] T. Nobukawa, K. Sugawara, K. Okumura, K. Tomishige, K. Kunimori, Appl. Catal. B: Environ. 70 (2007) 342.
[53] S. Brandenberger, O. Kröcher, A. Tissler, R. Althoff, Appl. Catal. A: Gen. 373 (2010) 168.
[54] A.A. Battiston, J.H. Bitter, W.M. Heijboer, F.M.F. de Groot, D.C. Koningsberger, J. Catal. 215 (2003) 279.
[55] U. Bentrup, A. Brückner, M. Richter, R. Fricke, Appl. Catal. B: Environ. 32 (2001) 229.
[56] A. Desikusumastuti, T. Staudt, M. Happel, M. Laurin, J. Libuda, J. Catal. 260 (2008) 315.
[57] T. Beutel, B.J. Adelman, W.M.H. Sachtler, Appl. Catal. B: Environ. 9 (1996) L1.
[58] D.D. Miller, S.S.C. Chuang, J. Phys. Chem. C 113 (2009) 14963.